CeO2 Nanoparticles-Loaded pH-Responsive Microparticles with Antitumoral Properties as Therapeutic Modulators for Osteosarcoma

ACS OMEGA

Article

Cite This: ACS Omega 2018, 3, 8952−8962

http://pubs.acs.org/journal/acsodf

CeO_2 Nanoparticles-Loaded pH-Responsive Microparticles with Antitumoral Properties as Therapeutic Modulators for Osteosarcoma

Christos Tapeinos,*[,†] Matteo Battaglini,[†,‡] Mirko Prato,[§] Gabriele La Rosa,[∥] Alice Scarpellini,[⊥] and Gianni Ciofani*[,†,#]

[†]Smart Bio-Interfaces, Istituto Italiano di Tecnologia, Viale Rinaldo Piaggio 34, 56025 Pontedera, PI, Italy

[‡]Scuola Superiore Sant'Anna, The Biorobotics Institute, Viale Rinaldo Piaggio 34, 56025 Pontedera, PI, Italy

[§]Materials Characterization Facility, [∥]Nanochemistry Department, and [⊥]Electron Microscopy Facility, Istituto Italiano di Tecnologia, Via Morego 30, 16163 Genova, Italy

[#]Department of Mechanical and Aerospace Engineering, Politecnico di Torino, Corso Duca degli Abruzzi 24, 10129 Torino, Italy

Supporting Information

ABSTRACT: Osteosarcoma is an aggressive form of bone cancer mostly affecting young people. To date, the most effective strategy for the treatment of osteosarcoma is the surgical removal of the tumor with or without combinational chemotherapy. In this study, we present the development of a pH-sensitive drug-delivery system in the form of microparticles, with increased chemotherapeutic action against the osteosarcoma cell line SAOS-2, and with reduced toxicity against the heart myoblastic cell line H9C2. The delivery system is composed of calcium carbonate and collagen type I, and is loaded with cerium dioxide (CeO_2) nanoparticles (<25 nm) and the anticancer drug doxorubicin. The fabricated microparticles were fully characterized morphologically and physicochemically, and their ability to induce or inhibit apoptosis/necrosis was assessed using in vitro functional assays and flow cytometry. The results presented in this study show that the highest concentration (250 μg/mL) of the therapeutic microparticles ($CaCO_3$-based therapeutic modulators (C-TherMods)), which corresponds to 6.4 μg/mL of encapsulated doxorubicin, can protect the H9C2 cells even after 120 h, since the percentage of viable cells at this time point is 65%. On the contrary, when H9C2 cells are treated with 0.5 μg/mL of free doxorubicin, 75% of the cells are dead only after 24 h. When SAOS-2 cells are treated with the same concentration of C-TherMods (250 μg/mL), the viability of SAOS-2 cells is 80% after 24 h, while it reduces to 50% after 120 h. At pH 6.0, the synergic effect of the pro-oxidant CeO_2 nanoparticles and of the encapsulated doxorubicin leads to almost 100% of cell death, even at the lowest concentration of C-TherMods (50 μg/mL).

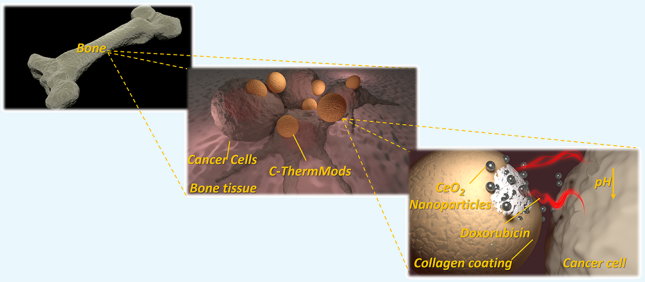

BACKGROUND

Osteogenic sarcoma (or osteosarcoma) is a form of malignant tumor that affects mostly young people below the age of 25 and elderly above the age of 60. It has a 5 year survival rate of 80%, which is dramatically reduced in the case of metastasis.[1−3] The current treatment for osteosarcoma comprises the use of chemotherapeutic drugs before the surgical removal of the tumor (neoadjuvant therapy), as well as after its removal (adjuvant therapy). The most common chemotherapeutic agents are doxorubicin (DOX), methotrexate, cisplatin, ifosfamide, and etoposide, as well as combinations of them. Although the use of these chemotherapeutics leads to a significant reduction of the tumor and an increase in the survival rate of the patients, it also leads to vital side effects, some of which are alopecia, myelosuppression, mucositis, nausea, and vomiting. Besides this, deaths due to acute toxicity have also been reported, especially in the case of DOX. More specifically, the toxic effects caused by DOX are related to the intensity and the total cumulative dose that is given to a patient, with a significant increase in heart failure when the administered dose is above 550 mg/m^2.[2,4]

Aiming at increasing the therapeutic effect and decreasing the side effects of the existing chemotherapeutics, various drug-delivery systems (DDS) based on organic and/or inorganic materials for the treatment of various types of cancer, as well as for other diseases, have been developed.[5−16] These systems allow for a better bioavailability, pharmacokinetics, controlled and sustained release of the encapsulated therapeutic agents, and specific targeting properties, those overall enhance the therapeutic efficacy of the administered drugs. Of the inorganic

Received: May 19, 2018
Accepted: July 30, 2018
Published: August 13, 2018

DOI: 10.1021/acsomega.8b01060
ACS Omega 2018, 3, 8952−8962

materials, the ones that are mostly used for the fabrication of DDS are gold, silicon, iron oxide, calcium phosphate, and calcium carbonate ($CaCO_3$).[17]

$CaCO_3$ in the form of microparticles, microspheres, and nanoparticles has been robustly used in drug delivery for the treatment of various types of cancer, including osteosarcoma, due to certain attractive characteristics such as its high biocompatibility, slow biodegradation, osteoconductivity, controlled and sustained release of various chemotherapeutics, and pH-sensitive properties.[17−21]

Collagen is one of the main components of the bone, along with bone minerals made mostly of calcium and phosphate salts. Collagen-based structures in the form of microspheres,[22] hydrogels,[23−25] and fibers[26,27] find use in many biomedical applications, such as drug-delivery systems for the treatment of cancer or applications related to tissue engineering, mostly due to the high biocompatibility and low immunogenicity that they present.

Overproduction of reactive oxygen species (ROS) is one of the main characteristics that cancerous tissues present, and recently, many studies that demonstrate reduction of malignant tumors through ROS up- or down-regulation have been published.[28,29] One of the materials that only recently has been started to be exploited for its dual ability to scavenge and to generate ROS according to alterations to the pH of the extra- and intracellular microenvironment is CeO_2. CeO_2 in the nanoscale range (e.g., nanoparticles) has the ability to scavenge ROS when the environmental pH is 7.4, yet generates reactive oxygen species when the pH is 6, a value close to the one that cancerous tissues present. This ability makes CeO_2 nanoparticles attractive since they can work as a natural bodyguard for healthy cells while selectively killing cancerous cells. On the basis of this, a number of studies that make use of CeO_2 nanoparticles alone or in combination with other types of treatments have been presented.[30,31]

In the scope of this, we hypothesized that the combination of CeO_2 nanoparticles and doxorubicin will reduce the toxicity of DOX towards healthy cells and will selectively kill cancer cells at lower pH values. We further hypothesized that the encapsulation of these nanoparticles inside a more stable delivery system that is not affected by the ionic strength of the microenvironment will increase its stability and release properties, allowing for an enhanced therapeutic efficacy. Thus herein, we present the development of pH-sensitive $CaCO_3$-based therapeutic modulators (C-TherMods) with enhanced anticancer properties for the potential treatment of osteogenic sarcoma. These microparticles, which are of spherical morphology, are composed of a calcium carbonate core and a thin layer of collagen type I, which acts as a barrier to the burst release of DOX through the C-TherMods. The C-TherMods which are loaded with CeO_2 nanoparticles (<25 nm) and with the anticancer drug DOX, aim at a reduction of the cytotoxicity on healthy heart cells (H9C2) and at an enhanced anticancer activity against osteosarcoma cells (SAOS-2) due to increased ROS generation at pH 6. The fabricated system was fully characterized morphologically and physicochemically, and loading and release studies were performed using high pressure liquid chromatography. The in vitro studies demonstrated that the combination of CeO_2 nanoparticles and DOX leads to an enhanced reduction in the proliferation of osteosarcoma (SAOS-2) cells, while at the same time protects against the toxicity toward heart cells (H9C2). The novelty of this study lies in the enhanced therapeutic activity of the C-TherMods due to the combinational treatment that it provides. Although other studies that make use of CeO_2 nanoparticles and/or DOX have been published, this is the first time that a system loaded with a therapeutic combination like the one described above is used, and that a simultaneous ability of inducing or inhibiting apoptosis/necrosis due to CeO_2 nanoparticles and DOX is presented.

MATERIALS AND METHODS

Materials. All of the materials were purchased from Sigma-Aldrich unless stated otherwise.

Preparation of $CaCO_3$ Therapeutic Modulators (C-TherMods). The calcium carbonate therapeutic modulators (C-TherMods) were fabricated using a simple co-precipitation method. In the first step, both $CaCl_2{\cdot}2H_2O$ (CAS: 10035-04-8) and Na_2CO_3 (CAS: 497-19-8) were dissolved in 400 and 300 μL of distilled water, respectively, while 10 mg of CeO_2 nanoparticles (<25 nm) (CAS: 1306-38-3) were dispersed in 100 μL of a doxorubicin (CAS: 25316-40-9) solution (10 mg/mL) in water. The dispersion of CeO_2 nanoparticles and doxorubicin were added to the Na_2CO_3 solution and vortexed for 30 s. The new dispersion (Na_2CO_3 + CeO_2 nanoparticles + doxorubicin) was added to the $CaCl_2$ solution under vigorous stirring (1500 rpm) and stirred for 30 s. Then, the dispersion was left to precipitate for 15 min and subsequently was washed three times with distilled water. The therapeutic microparticles were collected by centrifugation at 5000 rpm for 10 s.

The coating of the microparticles was performed at a second step. After cleaning, a small amount of the microparticles' dispersion was placed in a preweighted vial and freeze-dried to calculate the concentration of the dispersion. Then, the loaded microparticles were placed on a magnetic stirrer under normal stirring at pH 5.5, and collagen type I at the same pH and at a final concentration of 1.9 mg/mL was added to the dispersion. The new dispersion was stirred for 1 h and then the therapeutic modulators were centrifuged at 5000 rpm for 10 s and washed three times with distilled water. Then, the sample was freeze-dried and kept at 4 °C until further use.

Morphological and Physicochemical Characterization. *Electron Microscopy and Elemental Analysis.* The morphological characterization of the spherical microparticles was performed using a scanning electron microscope and a transmission electron microscope.

For the scanning electron microscopy (SEM) analysis, a FEI 200 operating at 15 keV, with beam currents varying from 43 pA to 0.17 nA, was used. The elemental analysis was performed using a built-in electron dispersion X-ray analysis detector from Bruker. All of the samples were coated with gold at 25 mA for 90 s before their study by SEM.

For the transmission electron microscopy (TEM) analysis, a FEI Tecnai G2 F20 TWIN TMP with a Schottky emitter operated at 200 kV was used. The energy-dispersive X-ray spectroscopy (EDS) analyses have been acquired using a Bruker XFlash 6|T30 silicon drift detector, with 30 mm^2 effective area. Each sample has been sonicated for a few minutes to avoid the presence of aggregates. The solution (5 μL) has been dropped onto an ultrathin carbon-coated Cu grid with a sample holder and a double-tilt analytical holder.

Dynamic Light Scattering (DLS). Dynamic light scattering measurements were performed using a Zetasizer Nano ZS90 of Malvern Instruments. The measurements before and after the collagen coating were carried out at 25 and 37 °C, and the

DOI: 10.1021/acsomega.8b01060
ACS Omega 2018, 3, 8952−8962

conductivity was adjusted in the range of 30−100 μS/cm using ultrapure water at a pH 5.5, to have comparable results.

The ζ potential values represent mean ± standard deviation (SD) of three different measurements and with 17 runs in each measurement. Before each acquisition, the samples were sonicated for ∼10 s using a Bandelin ultrasonic probe at 8 W to avoid the presence of aggregates.

Fourier Transform Infrared (FT-IR) Spectroscopy. Infrared spectroscopy was performed using a Shimadzu Miracle 10. Before the measurements, all of the samples have been freeze-dried. The number of scans was set to 45, the scanning range was set from 4000 to 400 cm^{-1}, and the resolution step was 4 cm^{-1}. The graphs were plotted using OriginPro software 9.1.

X-ray Photoelectron Spectroscopy (XPS) Analysis. XPS measurements were performed on a Kratos Axis Ultra DLD spectrometer using a monochromatized Al Kα source operating at 15 kV and 20 mA. Wide scans were acquired at an analyzer pass energy of 160 eV, while high-resolution narrow scans were performed at a constant pass energy of 10 eV and steps of 0.1 eV. The photoelectrons were detected at a takeoff angle $\Phi = 0°$ with respect to the surface normal. The pressure in the analysis chamber was maintained below 7×10^{-9} Torr for data acquisition. The data were converted to VAMAS format and processed using CasaXPS software, version 2.3.17. Data analysis on the Ce 3d energy region was performed to assess Ce(III) and Ce(IV) contents, following the method described in a previous study of our group.[32]

Inductively Coupled Plasma (ICP) Analysis. Inductively coupled plasma (ICP) atomic emission spectroscopy (AES) was performed using an iCAP 6500 Thermo spectrometer. All chemical analyses performed by ICP-AES were affected by a systematic error of about 5%. Samples were dissolved in HCl/HNO_3 3:1 (v/v).

Loading and Release Studies. The loading and release studies were performed using a high-performance liquid chromatograph (HPLC) Shimadzu LC-20AT. The chromatographic separation was carried out using a C-18 column (150 mm × 4.6 mm i.d., 5 μm particle size). The mobile phase consisted of acetonitrile and water (containing acetic acid 1%) and pumped in dynamic mode (gradient: ACN 15%-5 min, 25%-10 min, 50%-15 min, 75%-20 min) with a flow rate of 0.5 mL/min. The elution of the analyte was monitored at 480 nm. The standard curve was prepared by dissolving 1 mg of DOX in 1 mL of the mobile phase and filtered using a 0.2 μm syringe filter. A concentration range of 10−1000 μg/mL was obtained upon further serial dilution.

Antioxidant Capacity. The antioxidant ability of the final system (C-TherMods) was assessed using a total antioxidant capacity kit from Sigma-Aldrich according to manufacturer's instructions. Various concentrations of C-TherMods (50, 125, and 250 μg/mL) were tested, and the results were compared to the antioxidant capacity of Trolox, an analog of vitamin E.

In Vitro Studies. *Cell Lines.* In this study, two different cell lines were used, the osteogenic sarcoma cell line SAOS-2 (ATCC HTB-85) and the rat myoblastic cell line H9C2 (ATCC CRL-1446). Both cell lines were cultured in T75 flasks using high-glucose Dulbecco's modified Eagle's medium supplemented with 10% fetal bovine serum, 1% penicillin/streptomycin, and 1% L-glutamine, and at normal culture conditions (37 °C, 5% CO_2). For all of the experiments, the used cells were between passage 10 and passage 20. The medium during culture was changed every 2 days.

Metabolic Activity and Proliferation Assays. Upon 80% of confluence in a T75 flask, both cell lines were detached using trypsin 0.25% and seeded at a density of 25×10^3 cells/cm^2 in a 24-well tissue culture plate, with 500 μL of the same medium used for the culturing. After 48 h, the cells were treated with various concentrations of free doxorubicin (0.5, 1.0, 1.5, 3.0, and 6.0 μg/mL), free CeO_2 nanoparticles (12.5, 25, and 50 μg/mL), a combination of CeO_2 nanoparticles (50 μg/mL) and of the aforementioned doxorubicin concentrations, and with C-TherMods (50, 125, and 250 μg/mL). For H9C2, the pH of the used medium for all of the treatments was 7.4, while for SAOS-2, two different media, one at pH 7.4 and one at pH 6.0, were used. To assess the effect of each treatment on the cell metabolic activity and proliferation, a WST-1 assay (Sigma-Aldrich) and a Quant-iT PicoGreen dsDNA Assay Kit (Invitrogen) were used, respectively, according to the manufacturers' instructions. For the PicoGreen Assay Kit, 200 μL of Milli-Q ultrapure water was added to the cells, followed by scraping. The cell dispersion was frozen at −80 °C, and after three freeze−thaw cycles, a predetermined amount of the dispersion was used for DNA quantification. Sample fluorescence was measured using a PerkinElmer (Victor 2030) plate reader at λ_{ex} = 480 nm and λ_{em} = 520 nm.

Internalization Studies. To evaluate C-TherMods internalization, H9C2 and SAOS-2 cells were seeded on Ibidi 35 mm cell imaging Petri dishes and preincubated for 24 h with 100 μg/mL of particles in full supplemented media. After 24 h, the cells were washed two times with phosphate-buffered saline (PBS) solution and then fixed for 20 min at 4 °C with paraformaldehyde (4% in PBS). After the fixation, the cells were incubated for 30 min at room temperature with a blocking solution of goat serum (10% in PBS) and then stained for 30 min at 37 °C with a mixture of Oregon Green 488 Phalloidin 0.165 μM (Thermo Fisher) and Hoechst solution 5 μg/mL (Invitrogen). After staining, the cells were washed two times with PBS. The internalization of C-TherMods by cells was studied using confocal laser scanning microscopy on a Nikon $C2^+$ system (actin filament in green λ_{ex} = 488 nm, λ_{em} = 525 nm; C-TherMods in red λ_{ex} = 561 nm, λ_{em} = 585 nm; nuclei in blue λ_{ex} = 401 nm, λ_{em} = 447 nm). Three-dimensional (3D) rendering of *z*-stacks was performed by using NIS-Elements software (Nikon).

Assessment of Apoptosis/Necrosis. At predetermined time points (24, 72, and 120 h post-treatment), H9C2 and SAOS-2 (at pH 7.4 and 6.0) were trypsinized and incubated with annexin V-fluorescein isothiocyanate (FITC)/propidium iodide (PI) (Thermo Fisher) for viability, apoptosis, and cell death assessment by flow cytometry. Briefly, at each time point, cells were washed with Dulbecco's phosphate-buffered saline solution without calcium and magnesium and detached using trypsin−ethylenediaminetetraacetate (0.05%). A total of 100×10^3 cells per tube were stained with 2.5 μM annexin V-FITC and 1 μg/mL PI in annexin V binding buffer (1×) for 15 min at 37 °C protected from light. Cells stained with annexin V-FITC/PI were evaluated using a Beckman Coulter cytoflex. Live cells (annexin V−/PI−), apoptotic cells (annexin V+/PI−), and dead cells (PI+) were analyzed using Cytoflex software (Beckman Coulter). Untreated cells were used as controls.

RESULTS AND DISCUSSION

Morphological Characterization and Elemental Analysis. Calcium carbonate microspheres have been robustly used as antioxidant and/or as anticancer drug-delivery systems due to

DOI: 10.1021/acsomega.8b01060
ACS Omega 2018, 3, 8952−8962

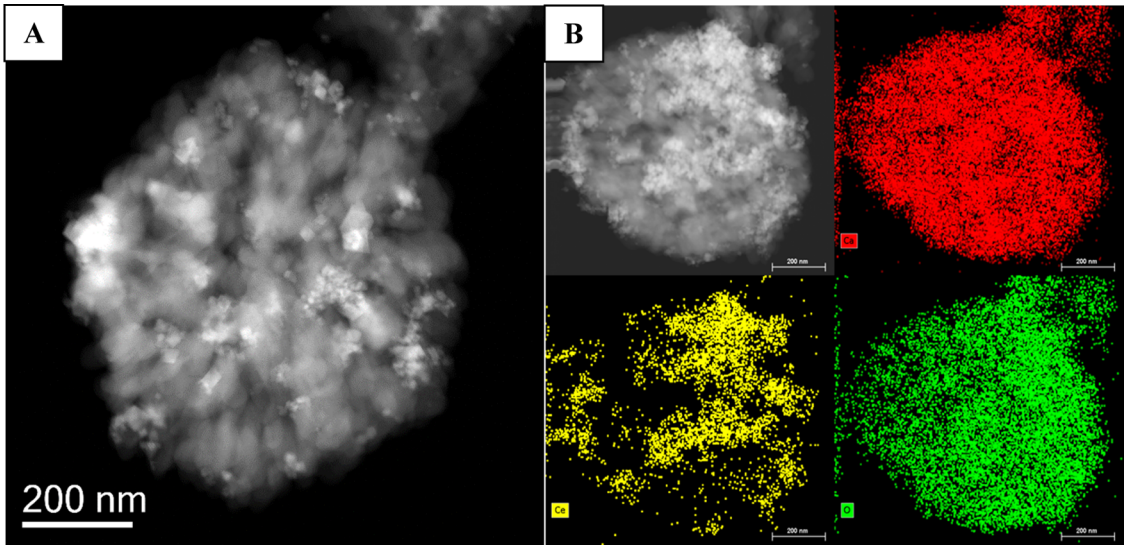

Figure 1. (A) Transmission electron micrograph of a C-TherMod and (B) EDS mapping of the elements that comprise C-TherMods (top right: Ca; bottom left: Ce; bottom right: O). The scale bar is 200 nm.

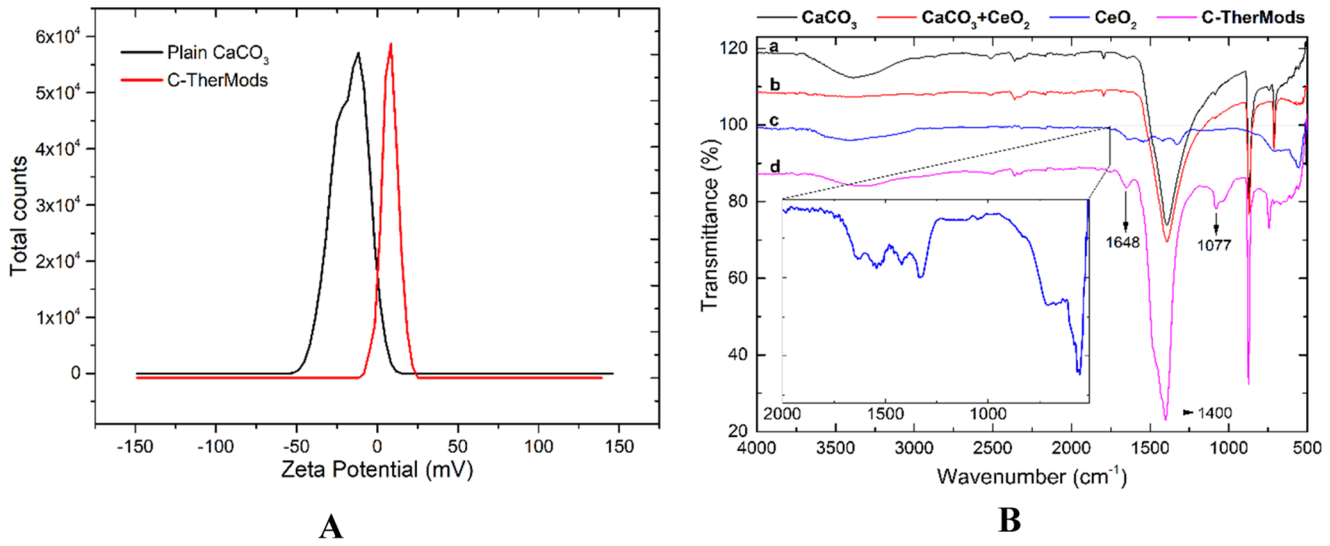

Figure 2. (A) ζ potential measurements of plain $CaCO_3$ microparticles ($\zeta = -20.90 \pm 2.12$ mV, cond. = 36.7 μS/cm) and C-TherMods ($\zeta = +11.80 \pm 5.91$ mV, cond. = 67.3 μS/cm) and (B) FT-IR spectra of plain $CaCO_3$ (spectrum a), $CaCO_3$ loaded with CeO_2 nanoparticles (spectrum b), free CeO_2 nanoparticles (spectrum c), and C-TherMods (spectrum d).

many advantages, including easy fabrication and pH-sensitive properties. However, although many studies related to $CaCO_3$-delivery systems loaded with antioxidant or anticancer drugs have been presented to date,[13,17,33] there has not been a study demonstrating that a calcium carbonate-based system can act as a modulator of oxidative stress and subsequently as a therapeutic modulator, by protecting healthy cells and killing cancer cells depending on the pH of the extracellular environment. In this study, we tried to combine the advantages of a calcium carbonate-delivery system with versatile CeO_2 nanoparticles, which can act as a pro-oxidant or as an antioxidant agent depending on the extracellular pH, and we also enhanced the therapeutic efficacy of our carrier toward osteosarcoma cells, by loading this carrier with the anticancer drug doxorubicin. In the final step, we coated the fabricated system with collagen aiming at attaching to the system a biomimetic character that mimics the bone environment.

After the synthesis, the first study that we performed was the morphological assessment of the calcium carbonate microparticles loaded with CeO_2 nanoparticles and doxorubicin and coated with collagen type I (hereafterin called C-TherMods), and this was carried out using transmission and scanning electron microscopy techniques. From the TEM and SEM images (Figures 1 and S1A in the Supporting Information), it can be seen that the microparticles consist of smaller particles creating a larger structure with a rough surface and an average size of 0.75 ± 0.25 μm (mean value of 100 particles). From the transmission electron micrograph, the presence of CeO_2 nanoparticles on the surface of C-TherMods is evident, and according to the XPS analysis presented in Figure S1B, the percentage of cerium (Ce) on the surface of the microparticles is 4.81% (other elements: C 47.44%, O 39.94%, Ca 7.17%, Na 0.64%). ICP analysis showed that the total percentage of Ce in the whole structure of C-TherMods is 17.70% (Ca: 36.80%). Mapping of the elements by energy-dispersive X-ray spectros-

DOI: 10.1021/acsomega.8b01060
ACS Omega 2018, 3, 8952−8962

copy (EDS, Figures 1 and S1A) and the EDS images presented in Figure S1C prove the homogeneous deposition of CeO_2 nanoparticles on the whole surface of the microparticles.

Physicochemical Characterization. To prove the successful coating with collagen as well as to further confirm the presence of CeO_2 nanoparticles, we performed dynamic light scattering measurements and Fourier transform infrared spectroscopy.

The ζ potential measurements demonstrated a negative surface charge (ζ) of the microparticles (-20.90 ± 2.12 mV) before collagen coating, while after the coating, a shift toward positive values ($+11.80 \pm 5.91$ mV) was observed, suggesting that collagen was successfully deposited on the surface of the $CaCO_3$ microparticles. This positive surface charge can be attributed to the amine and carboxylic groups of collagen, which at a slightly acidic pH (5.5) are protonated giving a positive ζ potential. The data presented in Figure 2A represent the average of three measurements at 25 °C, but similar results were also acquired when the temperature was increased at 37 °C.

Due to the fact that the CeO_2 nanoparticles on the surface of the microparticle may also affect the surface charge of the C-TherMods, we also performed infrared spectroscopy as a complementary technique to verify the presence of collagen. The data illustrated in Figure 2B present the spectra of (a) plain calcium carbonate microparticles ($CaCO_3$), (b) calcium carbonate microparticles loaded with CeO_2 nanoparticles ($CaCO_3$ + CeO_2), (c) commercial CeO_2 nanoparticles, and (d) collagen-coated calcium carbonate microparticles loaded with CeO_2 nanoparticles and DOX (C-TherMods). The strong broad peak at 1400 cm^{-1} in spectra (a), (b), and (d) corresponds to the v_3 asymmetric vibration of CO_3.[34] The peak at 1648 cm^{-1} in spectrum (d) can be attributed to the amide I (N−H) bond of collagen, while the peak at 1077 cm^{-1} corresponds to ν(C−O) and ν(C−O−C) absorptions of the carbohydrate moieties.[35] The peaks of CeO_2 in spectrum (c) (ca. 555 cm^{-1}, magnified spectrum) cannot be seen in spectrum (d) due to the weak signal that CeO_2 provides and due to the fact that these vibrations are covered by the strong vibrations of calcium carbonate at 1400 cm^{-1}. A magnified image of the peaks of CeO_2 (spectrum c) is also given in the inlet of Figure 2B, aiming at making more clear the presence of CeO_2 nanoparticles on C-TherMods.

The antioxidant ability of C-TherMods was finally studied and it was found that 50, 125, and 250 μg/mL of C-TherMods are equivalent with 20.0, 42.5, and 47.5 nmol of Trolox, respectively, proving their ability to scavenge ROS.

Loading and Release Studies. The dynamic loading, the encapsulation efficiency, and the release profiles of DOX encapsulated in C-TherMods at three different pH values (7.4, 6.0, and 4.5) were assessed by HPLC. From these studies, it was found that the encapsulation efficiency of C-TherMods is 88.40 ± 3.80%, while the dynamic loading was 2.56 ± 0.50%. The encapsulation efficiency values are close to other similar systems reported in the literature, where DOX is encapsulated inside calcium carbonate microparticles without any coating[36] or with a biomimetic coating,[37,38] as well as in systems where DOX is conjugated with CeO_2 nanoparticles.[39]

The release profile of DOX that is presented in Figure 3, demonstrates a controlled and sustained release over time, which depends on pH. At pH 7.4, the cumulative release of DOX reaches up to 18% after a period of 8 days, while this percentage is increased (35%) when the pH is reduced to 6.0 and further increases to 63% when the pH is further reduced to 4.5. It has to

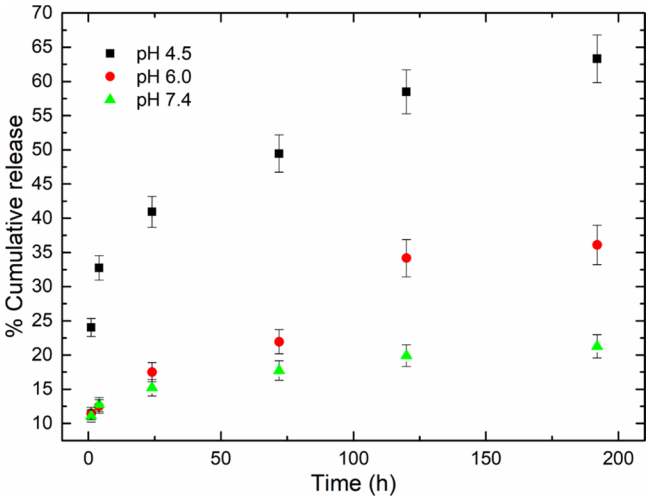

Figure 3. DOX release profiles from of C-TherMods acquired through HPLC at different time points (1, 4, 24, 72, 120, and 192 h) and at different pH values (4.5, 6.0, and 7.4) at 37 °C (data are presented as mean ± SD).

be noted that compared to other systems in the literature,[37] C-TherMods do not present a burst release in the first few hours inside the medium. This behavior may be attributed not only to the collagen layer around C-TherMods that is partially responsible for the slow release of DOX, but also due to potential electrostatic interactions between CeO_2 nanoparticles and DOX that further enhance this sustained release. It is also noteworthy that compared to other similar works in the literature, the release of DOX is slow and sustained when pH is 7.4, while it has a dramatic release when pH is 4.5. For example, Kamba et al. presented an 80% release of DOX at pH 7.4 after 20 h,[36] while Bosio et al.[38] and Dong et al.[37] presented at pH 7.4 a 50 and an 18% release after 24 h, respectively. During the release of DOX at lower pH, although the results demonstrated that the release behavior is similar to other systems, our system demonstrated a more controlled release depending on the pH, suggesting its appropriateness for controlled and sustained drug delivery.

When the pH is acidic, three parameters affect the release of DOX from the C-TherMods. The first one is the electrostatic interactions between amine and carboxylic groups of collagen, which start to protonate due to the low pH, leading to repulsion between the functional groups and potentially create some free space that allows the drug to be released. Secondly, the degradation of $CaCO_3$ at low pH also affects the release profile, while thirdly, as aforementioned, an increased release can also be potentially attributed to the alterations of the electrostatic interactions between CeO_2 nanoparticles and DOX.

Internalization Studies. Confocal microscopy was used to assess the ability of SAOS-2 and H9C2 to internalize the C-TherMods. The confocal images presented in Figure 4 prove that C-TherMods can be internalized from both cell lines after a period of 24 h. Complementary results from confocal microscopy can also be found in the Supporting Information (Figure S2).

Effect of Doxorubicin, CeO_2 Nanoparticles, and C-TherMods on Cell Proliferation. C-TherMods represent a stimuli-responsive and versatile system, the therapeutic ability of which depends on various constituents and conditions. In view of this, we assessed the effect of these various constituents on cell metabolic activity (Figure S3 in the Supporting Information)

DOI: 10.1021/acsomega.8b01060
ACS Omega 2018, 3, 8952−8962

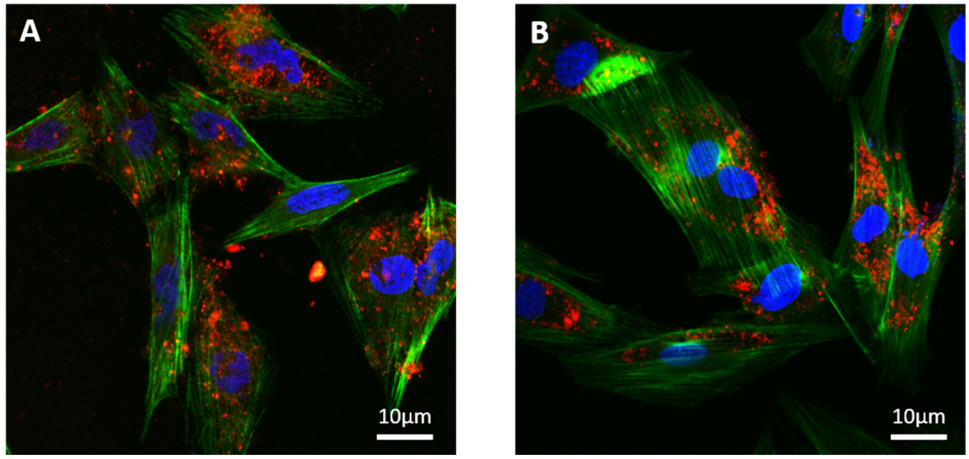

Figure 4. Internalization of C-TherMods (100 μg/mL) by (A) SAOS-2 and (B) H9C2 cells after 24 h of treatment (C-TherMods in red, F-actin in green, nuclei in blue).

and proliferation (Figure 5) independently, aiming at understanding how our system works. SAOS-2 was selected as an in vitro model for osteogenic sarcoma, and two different pH values were used, aimed at imitating the extra/intracellular pH of the environment of the tumor tissue. In addition, since the use of doxorubicin has been related to several side effects including a significant increase in heart failure depending on the administered dose, we used H9C2 as an in vitro model for studying the effect of C-TherMods on cardiac tissue. The results that are presented below as well as in the Supporting Information demonstrate that C-TherMods are not only able to kill cancer cells, but also in tandem protect H9C2 cells from the toxicity of doxorubicin.

It is evident from the graphs in Figure 5A−C that C-TherMods demonstrate a protective effect toward H9C2 in comparison to SAOS-2 (pHs 7.4 and 6.0) even at the lowest concentration for the first 24 h. The same protective effect can also be seen for the time points of 72 and 120 h (Figure 5A), although significantly different compared to the 24 h time point. The proliferation rate of H9C2 cells is reduced probably due to the release of doxorubicin that affects also the metabolic activity of H9C2. The proliferation rate of SAOS-2 at 72 h at both pH values (Figure 5B,C) is higher than the proliferation rate of H9C2, and this can be attributed to the fact that SAOS-2 are proliferating with a higher rate giving a higher proliferation compared to H9C2. This peculiarity can be seen only at the concentrations of 50 and 125 μg/mL of C-TherMods, probably due to the lower concentration of the encapsulated doxorubicin, while at the concentration of 250 μg/mL, the proliferation rate is similar for all cell types (Figure 5A−C, 250 μg/mL). At 120 h, it is more evident that C-TherMods at concentrations of 125 and 250 μg/mL provide higher protection to H9C2 (cell proliferation ∼65%) in comparison to SAOS-2 at pH 7.4 (cell proliferation ∼50%) and to SAOS-2 at pH 6.0 (cell proliferation ∼55%); for statistical significance, please see the corresponding figures. The presented results are in close agreement with the work of Zhao et al.,[33] in which a calcium carbonate/doxorubicin@silica nanoreactor was fabricated. In this study, the pH-dependent release of DOX affected the proliferation of HeLa cells in a dose- and time-dependent manner, resulting in an 80% reduction in cell proliferation after 24 h when 5 μg/mL of DOX was used and in a 40% reduction when DOX was encapsulated inside the proposed nanoreactor. These results are similar to the ones presented in this work, and more specifically with the results presented in Figure 5B (24 h) for 250 μg/mL of C-TherMods (corresponding to 6.4 μg/mL of free DOX) at pH 7.4, and with the results for free DOX that are presented in Figure 5H (3 and 6 μg/mL).

CeO_2 nanoparticles are well known for their enzyme-like activity, which allows them to act as a pro-oxidant (ROS generation) or as an antioxidant (ROS scavenging) depending on the pH. Taking into consideration this characteristic, and wanting to relate this property to the ability of C-TherMods to protect H9C2 cells and kill cancerous cells, we performed metabolic activity and DNA proliferation assays using various concentrations of CeO_2 nanoparticles. From the graphs depicted in Figure 5D−F, as well as from the graphs of metabolic activity (Figure S3D−F in the Supporting Information), it can be seen that CeO_2 nanoparticles do not have an effect either on the metabolic activity or on the proliferation of any of the treated cell lines. It was expected that CeO_2 nanoparticles at pH 6.0 would generate more ROS leading to a ROS-mediated apoptosis and to a reduction in the proliferation of SAOS-2, but as presented in Figure 5F, this is not evident. Two possible reasons can be hypothesized for the lack of any effect. The first reason is that CeO_2 nanoparticles at pH 6.0 do not generate a high amount of ROS capable of leading to ROS-mediated apoptosis, and the second one relies on a possible ability of SAOS-2 to scavenge the overproduced ROS. The high proliferation rate of SAOS-2 even at pH 6.0 leads to a high metabolic activity (Figure S3F in the Supporting Information) and an increased cell number, which can be responsible not only for increased ROS production, but also for increased ROS scavenging. Both the increased cell number due to high proliferation and the increased ROS scavenging support our aforementioned hypothesis.

In contrast to CeO_2 nanoparticles, doxorubicin presents cytotoxicity even at the lowest used concentration of 500 ng/mL (Figures 5G−I and S3G−I in the Supporting Information). According to the loading studies, the dynamic loading of doxorubicin is 2.56%, meaning that 50, 125, and 250 μg/mL of C-TherMods correspond to 1.28, 3.20, and 6.40 μg/mL of free doxorubicin. Comparing the results between free doxorubicin (Figures 5G−I and S3G−I in the Supporting Information) and C-TherMods (Figures 5A−C and S3A−C in the Supporting Information), it is pretty evident that C-TherMods provide protection toward H9C2 cells and a controlled cytotoxic effect over time toward SAOS-2 at pH values of 7.4 and 6.0 and at

DOI: 10.1021/acsomega.8b01060
ACS Omega 2018, 3, 8952−8962

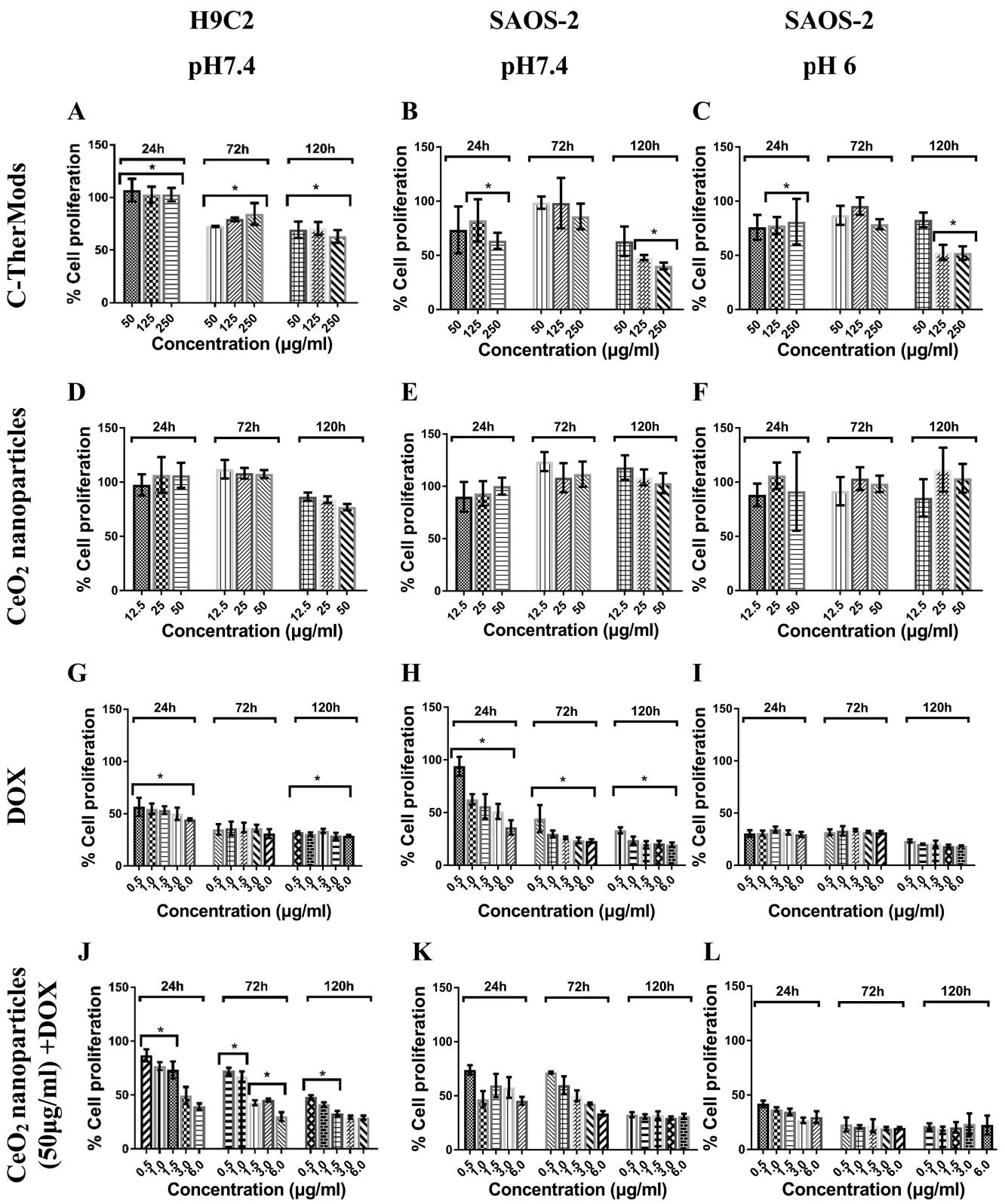

Figure 5. Proliferation of SAOS-2 and H9C2 cells after treatment with various concentrations of C-TherMods (A−C), CeO_2 nanoparticles (D−F), DOX (G−I), and a combination of CeO_2 nanoparticles and DOX (J−L) at different time points and at different pH values. Statistical analysis was performed using one-way analysis of variance, $*n = 3$, $p < 0.05$.

concentrations of 125 and 250 μg/mL (comparison between Figure 5A−C and 5G−I at 120 h and corresponding figures for metabolic activity, Figure S3A−C and S3G−I; for statistical significance, please see the corresponding figures).

To enhance our hypothesis concerning the protective role of CeO_2 nanoparticles inside C-TherMods, we have treated both SAOS-2 cells at pH values of 7.4 and 6.0 and H9C2 cells at pH 7.4 with C-TherMods that do not contain CeO_2 nanoparticles.

DOI: 10.1021/acsomega.8b01060
ACS Omega 2018, 3, 8952−8962

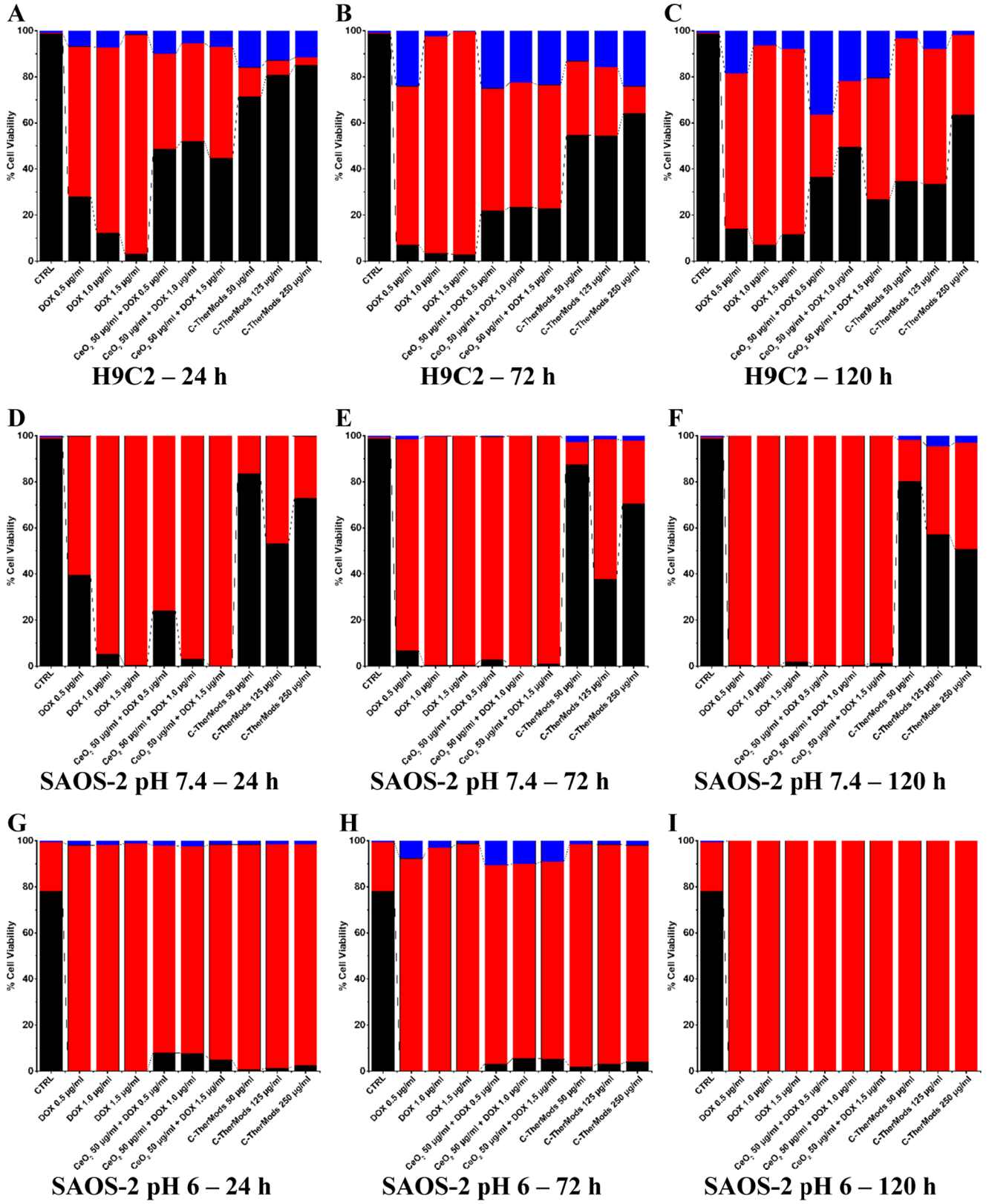

Figure 6. Bar graphs presenting % of live (black), necrotic (red), and apoptotic (blue) cells in H9C2 (A–C) and SAOS-2 cultures at pH 7.4 (D–F) and at pH 6.0 (G–I), after treatment with free DOX, a combination of CeO_2 nanoparticles + DOX, and C-TherMods for 24, 72, and 120 h. The samples coded as CTRL refer to untreated samples at 24 h, correspondingly for each condition (H9C2 at pH 7.4, SAOS-2 at pH 7.4, and SAOS-2 at pH 6.0).

Both the metabolic activity and the proliferation assays that are presented in the Supporting Information (Figure S4) show that even at the lowest concentration of C-TherMods (50 μg/mL) after 24 h, the metabolic activity of H9C2 cells is reduced to 75% (Figure S4A), while the cell proliferation (Figure S4D) is reduced to 30%, in contrast to C-TherMods that contain CeO_2

DOI: 10.1021/acsomega.8b01060
ACS Omega 2018, 3, 8952–8962

nanoparticles where the corresponding metabolic activity (Figure S3A) and the cell proliferation (Figure 5A) are 100%. It has to be noted that this difference in both the metabolic activity and cell proliferation can also be attributed to the different release profiles of DOX. As it is aforementioned, the release of DOX is also affected by the electrostatic interactions between CeO_2 nanoparticles and DOX, resulting in different release profiles in the presence or absence of CeO_2 nanoparticles. In the case of SAOS-2, a higher decrease in both metabolic activity (Figure S4B,C) and cell proliferation (Figure S4E,F) is observed after 24 h compared to the group where cells were treated with C-TherMods containing CeO_2 nanoparticles (Figures 5B,C and S3B,C). This behavior can be attributed to the faster release of DOX from C-TherMods, since as we mentioned before, the absence of CeO_2 nanoparticles possibly affects the release behavior. The protective role of CeO_2 nanoparticles inside C-TherMods is mostly evident after 72 h, when the cell proliferation in H9C2 is increasing with the concentration of C-TherMods if CeO_2 nanoparticles are encapsulated (Figure 5A), while decreasing with the increasing concentration of C-TherMods if CeO_2 nanoparticles are not used (Figure S4E). After 72 h, both H9C2 and SAOS-2 cells are dead probably due to the increased release of DOX.

Since CeO_2 nanoparticles did not present any cytotoxic effect even at the highest concentration of 50 μg/mL, and since doxorubicin presented a high cytotoxic effect even at the lowest concentration of 500 ng/mL, we decided to assess the effect that the combination of CeO_2 nanoparticles and doxorubicin can have. The results presented in Figures 5J−L and S3J−L demonstrate that the combination of CeO_2 nanoparticles and doxorubicin can have a protective effect as well as a cytotoxic effect depending on time and pH. In the case of H9C2 cells (Figure 5J), it is pretty evident that for the time point of 24 h and for concentrations of doxorubicin up to 1.5 μg/mL, CeO_2 nanoparticles can protect H9C2 cells. This protective effect can be attributed to the scavenging of overproduced ROS. Doxorubicin mechanism of action relies on the intercalation and inhibition of macromolecular anabolism, which stops the process of DNA replication. Along with this inhibition, doxorubicin can lead to cell apoptosis through ROS overproduction and a subsequent ROS-mediated apoptosis. We hypothesize that the protective effect that can be seen when CeO_2 nanoparticles and doxorubicin are combined is due to the fact that CeO_2 nanoparticles (ROS scavengers) counteract doxorubicin cytotoxic effect by reducing the ROS-mediated apoptosis. Although we cannot know the exact mechanism of action, the data presented in Figure 5J−L support our claims. At low doxorubicin concentrations, the protective effect is more evident and mostly for the H9C2 cells. When the concentration of doxorubicin is higher than 1.5 μg/mL, CeO_2 nanoparticles cannot protect H9C2 cells, thus leading to cell death (Figure 5J). The same protective effect can be seen also after 72 and 120 h (Figure 5J) with respect to free doxorubicin (Figure 5G). Comparing these data to the data about SAOS-2 at pH 7.4 (Figure 5K) and SAOS-2 at pH 6 (Figure 5L), we see that the protective effect of CeO_2 nanoparticles is not so evident in these cases. One possible reason for this is the pH value of SAOS-2 cultures: in the case of SAOS-2 at pH 6.0, we can assume that this slightly acidic pH either increases the ability of CeO_2 nanoparticles to produce ROS or reduces their ability to scavenge ROS.

Flow Cytometry—Apoptosis Studies. Flow cytometry was used as a complementary technique to assess the ability of C-TherMods to induce and/or to inhibit apoptosis. The results that are presented in Figure 6 and in Figure S5/Table S1 in the Supporting Information are in agreement with the results that were acquired using the dsDNA-based cell proliferation assay kit and that were analyzed above.

For the H9C2 cell line, it can be seen that the use of free DOX even at the lowest concentration of 0.5 μg/mL for 24 h (Figure 6A) leads to the death of H9C2 cells, with 65% of the cell population being necrotic and 7% being in the early apoptotic stage. As the concentration of DOX increases, the number of dead cells also increases to 80 and 95% for 1.0 and 1.5 μg/mL, respectively. When DOX is combined with CeO_2 nanoparticles at a concentration 50 μg/mL, it can be seen that the percentages of dead (necrotic) cells at 24 h are reduced to 49, 52, and 45%, for 0.5, 1.0, and 1.5 μg/mL, respectively, while the percentage of early apoptotic cells remains in the range of 7−10% (Figure 6A). This protective effect, as we pointed out in the previous paragraph, can be attributed to the therapeutic effect of CeO_2 nanoparticles. This protective effect is much higher when C-TherMods are used, not only due to the encapsulated CeO_2 nanoparticles, but also because of the slow release of doxorubicin, since at 24 h only 15% of DOX is released. Increased concentration of C-TherMods leads to an increased number of live cells, with 72, 81, and 85% viability for concentrations of 50, 125, and 250 μg/mL, respectively (Figure 6A). For these C-TherMods concentrations, the necrotic cells are, respectively, 13, 6, and 3%, while the early apoptotic cells are 16, 13, and 12%. The reason why early apoptosis is more evident in the cells treated with C-TherMods compared to free DOX and to the combination of CeO_2 nanoparticles and DOX, is attributed to the lower concentration of DOX that is released from the C-TherMods, allowing a better observation of apoptosis. After 72 h (Figure 6B), the majority (~90%) of H9C2 cells treated with free DOX are dead, while a small percentage (~23%) of the cells is alive when CeO_2 nanoparticles are used in combination with DOX. The viability of the cells is significantly higher when C-TherMods are used, presenting more than 50−60% viable H9C2 cells. After 120 h, the protective effect of C-TherMods is evident mostly at the highest concentration (250 μg/mL) of C-TherMods, where the viable cells remain at 65%, while for the lower concentrations the viability ranges approximately to 35% (Figure 6B).

In Figure 6D−F, results concerning SAOS-2 cells are different. When SAOS-2 cells are treated with free DOX or with the combination of CeO_2 nanoparticles + DOX, the majority of the cells is dead even at 24 h. When the SAOS-2 cells are treated with C-TherMods, the percentage of viable cells remains at 80% when the lowest concentration of C-TherMods (50 μg/mL) is used, ranges from 40 to 55% when 125 μg/mL is used, and reduces from 80% (24 h) to 50% (120 h) when 250 μg/mL are used. These results suggest that the cytotoxic effect of C-TherMods affects SAOS-2 cells in a dose-dependent manner, and also that this cytotoxicity is related to the controlled release of DOX. In addition, the DOX-related cytotoxicity can be counteracted by the protective ability of CeO_2 nanoparticles at pH 7.4, where they act as an antioxidant protecting the cells from ROS-mediated apoptosis. Finally, when the pH of the media is reduced to 6.0 (Figure 6G−I), 100% of the cells die after 24 h even after treatment with the lowest concentration of free DOX, CeO_2 nanoparticles + DOX, and C-TherMods. In these conditions, C-TherMods do not present any protective effect, and this could be attributed to the fact that CeO_2 nanoparticles start to act as pro-oxidants, leading to increased ROS and

DOI: 10.1021/acsomega.8b01060
ACS Omega 2018, 3, 8952−8962

enhancing the cytotoxic effect of the fabricated system through a combinatory ROS-mediated and DOX-mediated apoptosis. This hypothesis is supported by the work of Das et al.,[39] who present an enhanced antitumor effect against three different ovarian cancer cell lines when CeO_2 nanoparticles and DOX are combined, as well as by the work of Alpaslan et al.,[31] where it was demonstrated that a pH value around 6 enhances the cytotoxicity of CeO_2 nanoparticles and subsequently increases cell death in bone cancer cells, compared to physiological (7.0) and basic (9.0) pH values. It has to be noted that pH 6.0 is also affecting the viability of the cells, and this slightly acidic pH contributes to the increased cytotoxicity.

CONCLUSIONS

Herein, pH-responsive microparticles loaded with the anticancer drug doxorubicin and CeO_2 nanoparticles, and coated with collagen type I, were fabricated. These microparticles (C-TherMods) were fully characterized morphologically and physicochemically using several complementary material characterization techniques. The loading ability and the release profile of C-TherMods were assessed at various pH values, and it was found that C-TherMods can release DOX in a pH-dependent manner and over a period of time of more than 8 days. The in vitro studies using functional assays and the apoptosis/necrosis studies using flow cytometry demonstrated that C-TherMods have a protective effect toward the H9C2 heart myoblast cell line, and this protective effect could be attributed to the slow pH-dependent release of DOX as well as to the protective effect of CeO_2 nanoparticles. When C-TherMods were used to treat SAOS-2 at pH 7.4, it was found that their cytotoxic effect was dose-dependent, and after 120 h, the highest concentration of C-TherMods (250 μg/mL) led to a reduction of viable cells from 80% (24 and 72 h) to 51% (120 h). The protective effect of C-TherMods ceased to exist when the pH of the medium was reduced to 6, suggesting that the encapsulated CeO_2 nanoparticles started acting as pro-oxidants, enhancing in this way the cytotoxic effect of the C-TherMods by inducing cell death through a combination of ROS-mediated and DOX-mediated apoptosis.

The above-presented results suggest that the fabricated C-TherMods can act as novel stimuli-responsive therapeutic modulators able to protect specific cell lines (e.g., H9C2) and at the same time to kill the cancerous ones (e.g., SAOS-2).

ASSOCIATED CONTENT

Supporting Information

The Supporting Information is available free of charge on the ACS Publications website at DOI: 10.1021/acsomega.8b01060.

Material characterization data (SEM, XPS, and EDS); metabolic activity data; 3D confocal images of internalized C-TherMods; flow cytometry graphs; and a table presenting the date derived from the flow cytometry analysis (PDF)

AUTHOR INFORMATION

Corresponding Authors

*E-mail: christos.tapeinos@iit.it (C.T.).
*E-mail: gianni.ciofani@iit.it (G.C.).

ORCID

Christos Tapeinos: 0000-0001-8192-6750
Mirko Prato: 0000-0002-2188-8059
Gianni Ciofani: 0000-0003-1192-3647

Author Contributions

C.T. performed the synthesis and the morphological and physicochemical characterization of the material. The in vitro studies were carried out by C.T. and M.B. M.P. performed the XPS analysis, and G.L.R. conducted the ICP analysis. A.S. performed the transmission electron microscopy analysis. C.T. wrote the manuscript, which was edited and approved by all co-authors. C.T. and G.C. designed, supervised, and managed the study. All authors have given approval to the final version of the manuscript.

Notes

The authors declare no competing financial interest.

REFERENCES

(1) Botter, S. M.; Neri, D.; Fuchs, B. Recent advances in osteosarcoma. *Curr. Opin. Pharmacol.* **2014**, *16*, 15−23.
(2) Luetke, A.; Meyers, P. A.; Lewis, I.; Juergens, H. Osteosarcoma treatment - where do we stand? A state of the art review. *Cancer Treat. Rev.* **2014**, *40*, 523−532.
(3) Mirabello, L.; Troisi, R. J.; Savage, S. A. International osteosarcoma incidence patterns in children and adolescents, middle ages and elderly persons. *Int. J. Cancer* **2009**, *125*, 229−234.
(4) Janeway, K. A.; Grier, H. E. Sequelae of osteosarcoma medical therapy: a review of rare acute toxicities and late effects. *Lancet Oncol.* **2010**, *11*, 670−678.
(5) Tapeinos, C.; Battaglini, M.; Ciofani, G. Advances in the design of solid lipid nanoparticles and nanostructured lipid carriers for targeting brain diseases. *J. Controlled Release* **2017**, 306−332.
(6) Efthimiadou, E. K.; Tapeinos, C.; Chatzipavlidis, A.; Boukos, N.; Fragogeorgi, E.; Palamaris, L.; Loudos, G.; Kordas, G. Dynamic in vivo imaging of dual-triggered microspheres for sustained release applications: Synthesis, characterization and cytotoxicity study. *Int. J. Pharm.* **2014**, *461*, 54−63.
(7) Tapeinos, C.; Efthimiadou, E. K.; Boukos, N.; Charitidis, C. A.; Koklioti, M.; Kordas, G. Microspheres as therapeutic delivery agents: synthesis and biological evaluation of pH responsiveness. *J. Mater. Chem. B* **2013**, 194−203.
(8) Efthimiadou, E. K.; Tapeinos, C.; Bilalis, P.; Kordas, G. New approach in synthesis, characterization and release study of pH-sensitive polymeric micelles, based on PLA-Lys-b-PEGm, conjugated with doxorubicin. *J. Nanopart. Res.* **2011**, *13*, 6725−6736.
(9) Efthimiadou, E. K.; Tapeinos, C.; Tziveleka, L. A.; Boukos, N.; Kordas, G. PH- and thermo-responsive microcontainers as potential drug delivery systems: Morphological characteristic, release and cytotoxicity studies. *Mater. Sci. Eng., C* **2014**, *37*, 271−277.
(10) Tapeinos, C.; Pandit, A. Physical, Chemical, and Biological Structures based on ROS-Sensitive Moieties that are Able to Respond to Oxidative Microenvironments. *Adv. Mater.* **2016**, *28*, 5553−5585.
(11) Tapeinos, C.; Efthimiadou, E. K.; Boukos, N.; Kordas, G. Sustained release profile of quatro stimuli nanocontainers as a multi sensitive vehicle exploiting cancer characteristics. *Colloids Surf., B* **2016**, *148*, 95−103.
(12) Torchilin, V. P. Multifunctional, stimuli-sensitive nanoparticulate systems for drug delivery. *Nat. Rev. Drug Discovery* **2014**, *13*, 813−827.
(13) Larrañaga, A.; Mohd Isa, I. L.; Patil, V.; Thamboo, S.; Lomora, M.; Fernández-Yague, M. A.; Sarasua, J. R.; Palivan, C. G.; Pandit, A. Antioxidant Functionalized Polymer Capsules to Prevent Oxidative Stress. *Acta Biomater.* **2018**, 21−31.
(14) Genchi, G. G.; Marino, A.; Tapeinos, C.; Ciofani, G. Smart Materials Meet Multifunctional Biomedical Devices: Current and Prospective Implications for Nanomedicine. *Front. Bioeng. Biotechnol.* **2017**, *5*, 80.
(15) Zhang, Z.; Wang, F.; Balogh, D.; Willner, I. pH-controlled release of substrates from mesoporous SiO_2 nanoparticles gated by metal ion-dependent DNAzymes. *J. Mater. Chem. B* **2014**, *2*, 4449−4455.

DOI: 10.1021/acsomega.8b01060
ACS Omega 2018, 3, 8952−8962

(16) Chen, W.-H.; Yu, X.; Liao, W.-C.; Sohn, Y. S.; Cecconello, A.; Kozell, A.; Nechushtai, R.; Willner, I. ATP-Responsive Aptamer-Based Metal-Organic Framework Nanoparticles (NMOFs) for the Controlled Release of Loads and Drugs. *Adv. Funct. Mater.* **2017**, *27*, No. 1702102.
(17) Dizaj, S. M.; Barzegar-Jalali, M.; Zarrintan, M. H.; Adibkia, K.; Lotfipour, F. Calcium carbonate nanoparticles as cancer drug delivery system. *Expert Opin. Drug Delivery* **2015**, *12*, 1649−1660.
(18) Zhang, Y.; Ma, P.; Wang, Y.; Du, J.; Zhou, Q.; Zhu, Z.; Yang, X.; Yuan, J. Biocompatibility of Porous Spherical Calcium Carbonate Microparticles on Hela Cells. *World J. Nano Sci. Eng.* **2012**, *02*, 25−31.
(19) Biradar, S.; Ravichandran, P.; Gopikrishnan, R.; Goornavar, V.; Hall, J. C.; Ramesh, V.; Baluchamy, S.; Jeffers, R. B.; Ramesh, G. T. Calcium Carbonate Nanoparticles: Synthesis,Characterization and Biocompatibility. *J. Nanosci. Nanotechnol.* **2011**, *11*, 6868−6874.
(20) Liao, W. C.; Lilienthal, S.; Kahn, J. S.; Riutin, M.; Sohn, Y. S.; Nechushtai, R.; Willner, I. pH- and ligand-induced release of loads from DNA-acrylamide hydrogel microcapsules. *Chem. Sci.* **2017**, *8*, 3362−3373.
(21) Huang, F.; Liao, W. C.; Sohn, Y. S.; Nechushtai, R.; Lu, C. H.; Willner, I. Light-Responsive and pH-Responsive DNA Microcapsules for Controlled Release of Loads. *J. Am. Chem. Soc.* **2016**, *138*, 8936−8945.
(22) Tapeinos, C.; Larrañaga, A.; Sarasua, J.-R.; Pandit, A. Functionalised collagen spheres reduce H_2O_2 mediated. *Nanomedicine* **2017**, in press DOI: 10.1016/j.nano.2017.03.022.
(23) Cao, H.; Dong, Y.; Bre, L.; Tapeinos, C.; Wang, W.; Pandit, A. An acetal-based polymeric crosslinker with controlled pH-sensitivity. *RSC Adv.* **2016**, *6*, 9604−9611.
(24) Abu-Rub, M. T.; Billiar, K. L.; van Es, M. H.; Knight, A.; Rodriguez, B. J.; Zeugolis, D. I.; McMahon, S.; Windebank, A. J.; Pandit, A. Nano-textured self-assembled aligned collagen hydrogels promote directional neurite guidance and overcome inhibition by myelin associated glycoprotein. *Soft Matter* **2011**, *7*, 2770.
(25) Watanabe, K.; Nishio, Y.; Makiura, R.; Nakahira, A.; Kojima, C. Paclitaxel-loaded hydroxyapatite/collagen hybrid gels as drug delivery systems for metastatic cancer cells. *Int. J. Pharm.* **2013**, *446*, 81−86.
(26) Zeugolis, D. I.; Paul, G. R.; Attenburrow, G. Cross-linking of extruded collagen fibers–a biomimetic three-dimensional scaffold for tissue engineering applications. *J. Biomed. Mater. Res. A* **2009**, *89*, 895−908.
(27) Zeugolis, D. I.; Khew, S. T.; Yew, E. S.; Ekaputra, A. K.; Tong, Y. W.; Yung, L. Y.; Hutmacher, D. W.; Sheppard, C.; Raghunath, M. Electro-spinning of pure collagen nano-fibres - just an expensive way to make gelatin? *Biomaterials* **2008**, *29*, 2293−2305.
(28) Chen, Q.; Feng, L.; Liu, J.; Zhu, W.; Dong, Z.; Wu, Y.; Liu, Z. Intelligent Albumin-MnO_2 Nanoparticles as pH-/H_2O_2-Responsive Dissociable Nanocarriers to Modulate Tumor Hypoxia for Effective Combination Therapy. *Adv. Mater.* **2016**, *28*, 7129−7136.
(29) Prasad, P.; Gordijo, C. R.; Abbasi, A. Z.; Maeda, A.; Ip, A.; Rauth, A. M.; DaCosta, R. S.; Wu, X. Y. Multifunctional albumin-MnO(2) nanoparticles modulate solid tumor microenvironment by attenuating hypoxia, acidosis, vascular endothelial growth factor and enhance radiation response. *ACS Nano* **2014**, *8*, 3202−3212.
(30) Li, H.; Liu, C.; Zeng, Y. P.; Hao, Y. H.; Huang, J. W.; Yang, Z. Y.; Li, R. Nanoceria-Mediated Drug Delivery for Targeted Photodynamic Therapy on Drug-Resistant Breast Cancer. *ACS Appl. Mater. Interfaces* **2016**, *8*, 31510−31523.
(31) Alpaslan, E.; Yazici, H.; Golshan, N. H.; Ziemer, K. S.; Webster, T. J. pH-Dependent Activity of Dextran-Coated Cerium Oxide Nanoparticles on Prohibiting Osteosarcoma Cell Proliferation. *ACS Biomater. Sci. Eng.* **2015**, *1*, 1096−1103.
(32) Grillone, A.; Li, T.; Battaglini, M.; Scarpellini, A.; Prato, M.; Takeoka, S.; Ciofani, G. Preparation, Characterization, and Preliminary In Vitro Testing of Nanoceria-Loaded Liposomes. *Nanomaterials* **2017**, *7*, 276.
(33) Zhao, Y.; Luo, Z.; Li, M.; Qu, Q.; Ma, X.; Yu, S.-H.; Zhao, Y. A preloaded amorphous calcium carbonate/doxorubicin@silica nanoreactor for pH-responsive delivery of an anticancer drug. *Angew. Chem., Int. Ed.* **2015**, *54*, 919−922.
(34) Rodriguez-Blanco, J. D.; Shaw, S.; Benning, L. G. The kinetics and mechanisms of amorphous calcium carbonate (ACC) crystallization to calcite, via vaterite. *Nanoscale* **2011**, *3*, 265−271.
(35) Belbachir, K.; Noreen, R.; Gouspillou, G.; Petibois, C. Collagen types analysis and differentiation by FTIR spectroscopy. *Anal. Bioanal. Chem.* **2009**, *395*, 829−837.
(36) Kamba, S. A.; Ismail, M.; Hussein-Al-Ali, S. H.; Ibrahim, T. A.; Zakaria, Z. A. In vitro delivery and controlled release of Doxorubicin for targeting osteosarcoma bone cancer. *Molecules* **2013**, *18*, 10580−10598.
(37) Dong, Z.; Feng, L.; Zhu, W.; Sun, X.; Gao, M.; Zhao, H.; Chao, Y.; Liu, Z. $CaCO_3$ nanoparticles as an ultra-sensitive tumor-pH-responsive nanoplatform enabling real-time drug release monitoring and cancer combination therapy. *Biomaterials* **2016**, *110*, 60−70.
(38) Bosio, V. E.; Cacicedo, M. L.; Calvignac, B.; Leon, I.; Beuvier, T.; Boury, F.; Castro, G. R. Synthesis and characterization of $CaCO_3$-biopolymer hybrid nanoporous microparticles for controlled release of doxorubicin. *Colloids Surf., B* **2014**, *123*, 158−169.
(39) Das, J.; Choi, Y. J.; Han, J. W.; Reza, A.; Kim, J. H. Nanoceria-mediated delivery of doxorubicin enhances the anti-tumour efficiency in ovarian cancer cells via apoptosis. *Sci. Rep.* **2017**, *7*, No. 9513.

DOI: 10.1021/acsomega.8b01060
ACS Omega 2018, 3, 8952−8962